

STEADY STATE AXISYMMETRIC DEFORMATIONS OF A THERMOVISCOPLASTIC ROD STRIKING A HEMISPHERICAL RIGID CAVITY

R. C. BATRA and PEI-RONG LIN

Department of Mechanical and Aerospace Engineering and Engineering Mechanics,
University of Missouri–Rolla, Rolla, MO 65401-0249, U.S.A.

(Received 13 May 1988; and in revised form 9 November 1988)

Summary—Steady state thermomechanical deformations of a semi-infinite rod moving at a very high speed and hitting a rigid hemispherical cavity are studied. It is assumed that the deformations of the rod are axisymmetric, that its material can be modeled as rigid–viscoplastic, that the material exhibits work-hardening, strain-rate hardening and thermal softening effects, and that the contact between the deforming rod and the cavity surface is smooth. It is found that the axial force experienced by the rod depends strongly upon its speed. An effort has been made to identify the effect of work hardening, strain-rate hardening and thermal softening on the deformations of the rod. Results computed and presented graphically include the distribution of the velocity field, the temperature change, the second-invariant of the strain-rate tensor and the principal stresses in the deforming region. Also plotted are the normal tractions on the cavity wall.

NOTATION

v	velocity of a rod particle
ρ	mass density
q	heat flux
U	specific internal energy
D	strain-rate tensor
σ	Cauchy stress tensor
s	deviatoric stress tensor
p	hydrostatic pressure
θ	temperature change
k	thermal conductivity
c	specific heat
σ_0	yield stress in simple compression
b, m	strain-rate sensitivity parameters
γ	thermal softening coefficient
ψ_0, n	work-hardening parameters
t	a unit tangent vector
n	a unit normal vector
h, \bar{h}	heat transfer coefficient

1. INTRODUCTION

A widely used approach in analyzing the penetration of a fast moving (speed $\geq 1 \text{ km s}^{-1}$) projectile into a very thick target assumes that the deformations of the target and the projectile are governed by purely hydrodynamic incompressible flow processes. Thus, the only material property of significance is the ratio of mass densities of the target and the penetrator. Since this theory predicts the same penetration depth for all impact velocities, Tate [1, 2] and Alekseevskii [3] modified this model by including the effects of the material strengths of the projectile and the target. They assumed the material strength to be some multiple of the uniaxial yield stress of the material, but the multiplying factor is unresolved within the context of these theories. Since these theories are one-dimensional, they ignore the lateral motion, plastic flow and detailed dynamic effects. These and other limitations of the one-dimensional models have been lucidly discussed by Wright [4]. An authoritative and superb review of the open literature on ballistic penetration, containing 278 reference

citations from 1800s until 1977, is the paper by Backman and Goldsmith [5]. It describes different physical mechanisms involved in the penetration and perforation processes, and also discusses a number of engineering models. The reader is also referred to the recent review of the status of ballistic impact modeling by Anderson and Bodner [6]. Penetration models that are not very difficult to use have been proposed by Ravid and Bodner [7] and Ravid, Bodner and Holcman [8]. The model proposed in [7] is two-dimensional, utilizes five penetration stages, is applicable to rigid projectiles and presumes a kinematically admissible flow field in the target. Various unknown parameters appearing in the presumed flow field are found by using an upper bound theorem of plasticity modified to include dynamic effects. The penetration model proposed by Ravid, Bodner and Holcman also accounts for the shock effects and plastic deformation in the component bodies.

In an attempt to understand better the approximations made in simple theories of penetration [1–3] and to provide some guidelines for improving kinematically admissible fields in engineering models of penetration, Batra and Wright [9] embarked upon studying an idealized steady state penetration problem. In it, they assumed that the rod is semi-infinite in length, that the target is infinite with a semi-infinite hole, that the rate of penetration and all flow fields appear steady to an observer situated on the penetrator nose and that the target/penetrator interface is smooth. They studied the problem of the deformable target, presumed to be made of a rigid–perfectly plastic material, and a rigid penetrator having a circular cylindrical body with a hemispherical nose. Subsequently, Batra [10, 11] analyzed the problem for different penetrator nose shapes and accounted for work-hardening, strain-rate hardening and thermal softening of the target material.

Batra and Lin [12] have recently studied the steady state axisymmetric deformations of a semi-infinite cylindrical penetrator striking a known semi-infinite cavity in an infinite and rigid target. This problem is more challenging than the companion problem analyzed in [9–11] because of the presence in it of a free surface whose shape is not known *a priori*. Batra and Lin's calculations revealed that peak strain-rates in the range 10^5 – 10^6 s⁻¹ invariably occurred at or near the bottom-most point of the free surface. Since many materials used for high energy penetrators have strain-rate sensitive properties, we extend herein the previous work [12] to viscoplastic materials that exhibit thermal softening too. The effect of work hardening of the material is accounted for by the use of an internal variable whose rate of evolution is proportional to the plastic working.

We note that there is no fracture or failure criterion incorporated in our work. Thus the material is presumed to undergo unlimited plastic deformations. Nevertheless, the kinematic, kinetic and temperature fields found herein should help in proposing and/or checking results from simpler engineering theories of penetration.

2. FORMULATION OF THE PROBLEM

We use a cylindrical coordinate system, with the origin at the bottom of the hemispherical cavity in an infinite rigid target and z -axis pointing out of the cavity, to describe the steady-state axisymmetric deformations of the cylindrical penetrator striking the cavity. We assume that the axes of the penetrator and the cavity coincide with each other. The governing field equations are

$$\operatorname{div} \mathbf{v} = 0, \quad (1)$$

$$\operatorname{div} \boldsymbol{\sigma} = \rho \dot{\mathbf{v}}, \quad (2.1)$$

$$= \rho(\mathbf{v} \cdot \operatorname{grad})\mathbf{v}, \quad (2.2)$$

$$-\operatorname{div} \mathbf{q} + \operatorname{tr}(\boldsymbol{\sigma} \mathbf{D}) = \rho(\mathbf{v} \cdot \operatorname{grad})U, \quad (3)$$

$$2\mathbf{D} = \operatorname{grad} \mathbf{v} + (\operatorname{grad} \mathbf{v})^T. \quad (4)$$

Equations (1)–(3), written in the Eulerian description of motion, express the balance of mass, balance of linear momentum and balance of internal energy, respectively. Here, \mathbf{v} is the velocity of a rod particle, $\boldsymbol{\sigma}$ the Cauchy stress, \mathbf{q} the heat flux, ρ the mass density and

U the specific internal energy; a dot over a character denotes the material time differentiation, and the operators grad and div signify the gradient and the divergence operators on fields defined in the present configuration. In equation (1) we have assumed that the deformations are isochoric, and in equation (3) that all of the plastic working, rather than the 90–95% of it asserted by Farren and Taylor [13], is converted into heat. Equations (1)–(3) ought to be supplemented by constitutive relations and boundary conditions.

For the constitutive relations, which are characteristic of the penetrator material, we take

$$\mathbf{q} = -k \text{ grad } \theta, \quad (5)$$

$$U = c\theta, \quad (6)$$

$$\boldsymbol{\sigma} = -p\mathbf{1} + 2\mu(I, \theta, \psi)\mathbf{D}, \quad \text{whenever } \mathbf{D} \neq \mathbf{0}, \quad (7)$$

$$\mathbf{D} = \mathbf{0} \quad \text{if } \text{tr}(\mathbf{s}^2) < \frac{2}{3} \sigma_0^2 (1 - \gamma\theta)^2 \left(1 + \frac{\psi}{\psi_0}\right)^{2n}, \quad (8)$$

$$\mathbf{s} \equiv \boldsymbol{\sigma} + p\mathbf{1}, \quad (9)$$

$$2\bar{\mu}(I, \theta, \psi) = \frac{\sigma_0}{\sqrt{3}I} (1 + bI)^m (1 - \gamma\theta) \left(1 + \frac{\psi}{\psi_0}\right)^n, \quad (10)$$

$$\dot{\psi} = (\mathbf{v} \cdot \text{grad})\psi = \text{tr}(\boldsymbol{\sigma}\mathbf{D}) \left/ \left(1 + \frac{\psi}{\psi_0}\right)^n \right., \quad (11)$$

$$2I^2 \equiv \text{tr}(\mathbf{D}^2). \quad (12)$$

In these equations k is the thermal conductivity, c the specific heat, θ the temperature change of a material particle from that in the reference configuration (θ_0), p the hydrostatic pressure not determined from the strain-rate field \mathbf{D} because of the assumption of incompressibility of the material, σ_0 the yield stress in quasistatic simple tension or compression test, and ψ , whose growth is governed by equation (11), is an internal variable used to describe the work-hardening of the material. The material parameters b and m define how the flow stress depends upon the strain-rate, ψ_0 and n characterize the dependence of the flow stress upon the work-hardening, and γ is the inverse of $(\theta_m - \theta_0)$ where θ_m is the melting temperature of the penetrator material. That the flow stress decreases linearly with the temperature rise has been observed by Bell [14] and Lindholm and Johnson [15]. Of course, the range of temperatures investigated by Bell and by Lindholm and Johnson is not as large as that likely to occur here. Rosenberg *et al.* [16] observed that for C1008 steel the stress at 10% strain in simple compression decreases linearly when the temperature is increased from 25°C to 500°C, and stays constant from 500°C to 700°C. Other investigators, e.g. Costin *et al.* [17], have reported a power law dependence of the flow stress upon the temperature. In writing equation (7), we have neglected the elastic deformations of the penetrator. Equations (7), (9) and (10) imply that

$$\left(\frac{1}{2} \text{tr } \mathbf{s}^2\right)^{1/2} = \frac{\sigma_0}{\sqrt{3}} (1 + bI)^m (1 - \gamma\theta) \left(1 + \frac{\psi}{\psi_0}\right)^n, \quad (13)$$

which can be viewed as a generalized von Mises yield criterion when the flow stress, given by the right-hand side of equation (13), at a material particle depends upon its strain-rate, strain and temperature. Zienkiewicz *et al.* [18] used a similar approach and took

$$2\mu = [\sigma_0 + (2I/\sqrt{3}\hat{\psi})^{1/n}]/\sqrt{3}I,$$

where $\hat{\psi}$ and n are functions of θ . They asserted that it represents Perzyna's viscoplastic model. Tate [19] considered the effect of thermal softening only and used equation (7) with $m = n = 0$ in equation (10). Batra [11], who also used equation (7) to study the steady-state thermomechanical deformations of a target being penetrated by a rigid cylindrical rod, has discussed the relation of equation (7) to other constitutive relations.

Finally, we note that equation (7) may be interpreted as a constitutive relation for a non-Newtonian fluid whose viscosity μ depends upon the strain-rate, temperature and material parameter ψ .

For the boundary conditions on the rod/cavity interface, we take

$$\mathbf{t} \cdot (\boldsymbol{\sigma}\mathbf{n}) = 0, \quad (14)$$

$$\mathbf{v} \cdot \mathbf{n} = 0, \quad (15)$$

$$\mathbf{q} \cdot \mathbf{n} = h(\theta - \theta_a), \quad (16)$$

where h is the heat transfer coefficient between the rod and target materials and \mathbf{n} and \mathbf{t} are, respectively, a unit normal and a unit tangent vector. Note that \mathbf{n} points into the rigid target and θ_a is the average temperature of the target material. The boundary condition (14) represents smooth contact between the rod and the target, and equation (15) implies that rod particles do not penetrate into the rigid target. The boundary condition (14) appears reasonable, since a thin layer of material at the interface either melts or is severely degraded by adiabatic shear. On the free surface of the rod,

$$\boldsymbol{\sigma}\mathbf{n} = 0, \quad (17)$$

$$\mathbf{v} \cdot \mathbf{n} = 0, \quad (18)$$

$$\mathbf{q} \cdot \mathbf{n} = \tilde{h}(\theta - \tilde{\theta}), \quad (19)$$

where \mathbf{n} is a unit outward normal to the surface, \tilde{h} is the heat transfer coefficient between the rod material and air and $\tilde{\theta}$ is the air temperature. The boundary condition (18) ensures that the velocity of particles on the free surface is tangent to the surface. We note that the boundary condition (18) is not needed for the complete specification of the problem, provided that the shape of the free surface is known. Since this is not the case here, condition (18) is used to test whether or not the presumed shape of the free surface is correct.

On the rod cross-section far from the cavity bottom,

$$|\mathbf{v} + v_0\mathbf{e}_z| \rightarrow 0, \quad |\theta - \tilde{\theta}| \rightarrow 0 \quad \text{as } z \rightarrow \infty; \quad (20)$$

on the deformed rod material at the cavity outlet,

$$|\boldsymbol{\sigma}\mathbf{n}| \rightarrow 0, \quad |\mathbf{q} \cdot \mathbf{n}| \rightarrow 0 \quad \text{as } (r^2 + z^2)^{1/2} \rightarrow \infty. \quad (21)$$

Equation (20) states that the end of the rod far from the cavity bottom is moving with a uniform speed v_0 in the positive z -direction and is at a uniform temperature $\tilde{\theta}$. According to equation (21), at the cavity outlet, the rod particles are traction free and there is no heat exchange between them and the material on the other side of the outlet surface. A precise statement of equations (20) and (21) will involve the specification of the rates of decay of the field quantities. However, at this time, there is little hope of proving any existence or uniqueness theorem for the stated problem and we therefore gloss over this rather touchy issue. Herein we assume that there exists a solution to the problem defined by equations (1)–(12) and (14)–(21), and seek an approximation to that solution by the finite element method.

The introduction of non-dimensional variables, indicated in equation (22) by bars over characters, will help in the analysis of the problem over a broad range of values of various parameters:

$$\begin{aligned} \bar{\boldsymbol{\sigma}} &= \boldsymbol{\sigma}/\sigma_0, & \bar{p} &= p/\sigma_0, & \bar{\mathbf{s}} &= \mathbf{s}/\sigma_0, & \bar{\mathbf{v}} &= \mathbf{v}/v_0, & \bar{r} &= r/r_0, & \bar{z} &= z/r_0, \\ \bar{\theta} &= \theta/\theta_0, & \bar{b} &= bv_0/r_0, & \bar{\gamma} &= \gamma\tilde{\theta}_0, & \alpha &= \rho v_0^2/\sigma_0, & & & & \\ \beta &= k/(\rho c v_0 r_0), & \bar{\theta}_0 &\equiv \sigma_0/(\rho c), & \bar{h} &= h/(\rho c v_0). \end{aligned} \quad (22)$$

Substituting from equations (5)–(10) into equations (1)–(3) and (11), rewriting these in terms of non-dimensional variables, denoting the gradient and divergence operators in non-dimensional coordinates by grad and div , and dropping the bars, we arrive at the

following set of equations:

$$\operatorname{div} \mathbf{v} = 0, \quad (23)$$

$$\operatorname{div} \boldsymbol{\sigma} = \alpha(\mathbf{v} \cdot \operatorname{grad}) \mathbf{v}, \quad (24)$$

$$\operatorname{tr}(\boldsymbol{\sigma} \mathbf{D}) + \beta \operatorname{div}(\operatorname{grad} \theta) = (\mathbf{v} \cdot \operatorname{grad}) \theta, \quad (25)$$

$$\operatorname{tr}(\boldsymbol{\sigma} \mathbf{D}) \left/ \left(1 + \frac{\psi}{\psi_0} \right)^n \right. = (\mathbf{v} \cdot \operatorname{grad}) \psi, \quad (26)$$

where

$$\boldsymbol{\sigma} = -p \mathbf{1} + \frac{1}{\sqrt{3}I} (1 + bI)^m (1 - \gamma\theta) \left(1 + \frac{\psi}{\psi_0} \right)^n \mathbf{D}. \quad (27)$$

The boundary conditions (14)–(21) when written in terms of non-dimensional variables look exactly the same. Hereafter we shall use non-dimensional variables only.

3. FINITE ELEMENT FORMULATION OF THE PROBLEM

We note that a numerical solution of the problem requires that we consider a finite region and know the shape of the free surface. We presume the latter and study deformations of the rod over the region R shown in Fig. 1, which also depicts a spatial discretization of R . The iterative procedure used to check whether or not the assumed shape of the free surface is correct and to modify it if necessary has been described by Batra and Lin [12]. The adequacy of the finite domain studied will be verified by solving the problem for two separate regions, one of them larger and containing the other, and ensuring that the two sets of computed values of various field quantities are close to each other.

The boundary conditions (14)–(16) and (17)–(19) apply on the cavity surface BC and the free surface FED, respectively. Equations (20) and (21) are replaced by the equations

$$v_z = -1.0, \quad v_r = 0, \quad \theta = 0 \quad \text{on AF}, \quad (28)$$

$$\mathbf{v} = v_e \mathbf{n}, \quad \mathbf{t} \cdot (\boldsymbol{\sigma} \mathbf{n}) = 0, \quad \mathbf{q} \cdot \mathbf{n} = 0 \quad \text{on the outlet surface CD} \quad (29)$$

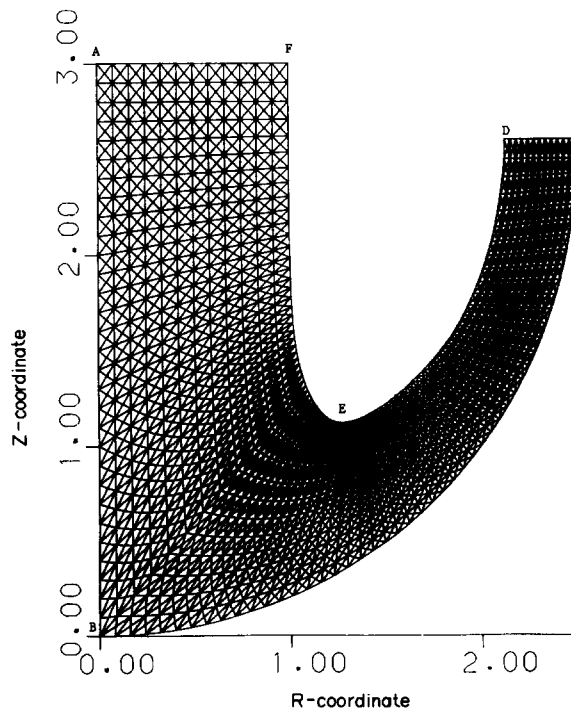


FIG. 1. The finite region studied and its spatial discretization.

and we impose

$$\sigma_{rz} = 0, \quad v_r = 0, \quad \frac{\partial \theta}{\partial r} = 0 \quad (30)$$

on the axis of symmetry AB. When a shape of the free surface has been presumed, the value of v_e is computed so as to satisfy the balance of mass.

The details of the derivations of a weak formulation of the problem are given in several books—see for example Becker *et al.* [20], Zienkiewicz [21] and Hughes [22]. We omit the details, and simply state that a weak formulation of the problem defined on the region R by equations (23)–(26) and boundary conditions (14)–(19) and (28)–(30) is that equations

$$\int_R \lambda(\operatorname{div} \mathbf{v}) dV = 0, \quad (31)$$

$$\int_R p(\operatorname{div} \boldsymbol{\phi}) dV - \int_R \mu(I, \theta, \psi)[\mathbf{D} : (\operatorname{grad} \boldsymbol{\phi} + (\operatorname{grad} \boldsymbol{\phi})^T)] dV = \alpha \int [(\mathbf{v} \cdot \operatorname{grad}) \mathbf{v}] \cdot \boldsymbol{\phi} dV, \quad (32)$$

$$\begin{aligned} \int_R [(\mathbf{v} \cdot \operatorname{grad}) \theta] \eta dV + \beta \int_R \operatorname{grad} \theta \cdot \operatorname{grad} \eta dV + h \int_{\partial_1 R} \theta \eta dA + \tilde{h} \int_{\partial_2 R} \theta \eta dA \\ = \int_R \eta(\boldsymbol{\sigma} : \mathbf{D}) dV - h \int_{\partial_1 R} \theta_a \eta dA - \tilde{h} \int_{\partial_2 R} \theta \eta dA, \end{aligned} \quad (33)$$

$$\int_R [(\mathbf{v} \cdot \operatorname{grad}) \psi] \xi dV = \int_R \frac{(\boldsymbol{\sigma} : \mathbf{D}) \xi}{\left(1 + \frac{\psi}{\psi_0}\right)^n} dV, \quad (34)$$

hold for arbitrary smooth functions λ , $\boldsymbol{\phi}$, η and ξ defined on R such that $\phi_r = 0$ on AF and AB, $\phi_z = 0$ on AF, $\boldsymbol{\phi} \cdot \mathbf{n} = 0$ on FED and DC and $\eta = 0$ on AF. In these equations $\mathbf{A} : \mathbf{B} = \operatorname{tr}(\mathbf{A}\mathbf{B}^T)$ for linear transformations \mathbf{A} and \mathbf{B} , $\partial_1 R$ is the surface BC and $\partial_2 R$ denotes the free surface FED. The nonlinear equations (31)–(34) are solved iteratively for \mathbf{v} , θ and ψ . At the i th iteration, equations

$$\int_R \lambda(\operatorname{div} \mathbf{v}^i) dV = 0, \quad (35)$$

$$\begin{aligned} \int_R p^i(\operatorname{div} \boldsymbol{\phi}) dV - \int_R \mu(I^{i-1}, \theta^{i-1}, \psi^{i-1})[\mathbf{D}^i : (\operatorname{grad} \boldsymbol{\phi} + (\operatorname{grad} \boldsymbol{\phi})^T)] dV \\ = \alpha \int_R [(\mathbf{v}^{i-1} \cdot \operatorname{grad}) \mathbf{v}^i] \cdot \boldsymbol{\phi} dV, \end{aligned} \quad (36)$$

$$\begin{aligned} \int_R [(\mathbf{v}^{i-1} \cdot \operatorname{grad}) \theta^i] \eta dV + \beta \int_R \operatorname{grad} \theta^i \cdot \operatorname{grad} \eta dV + h \int_{\partial_1 R} \theta^i \eta dA + \tilde{h} \int_{\partial_2 R} \theta^i \eta dA \\ = \int_R \eta(\boldsymbol{\sigma}^{i-1} : \mathbf{D}^{i-1}) dV - h \int_{\partial_1 R} \theta_a \eta dA - \tilde{h} \int_{\partial_2 R} \theta \eta dA, \end{aligned} \quad (37)$$

$$\int_R [(\mathbf{v}^{i-1} \cdot \operatorname{grad}) \psi^i] \xi dV = \int_R \frac{\boldsymbol{\sigma}^{i-1} : \mathbf{D}^{i-1}}{\left(1 + \frac{\psi}{\psi_0}\right)^n} \xi dV \quad (38)$$

are solved for \mathbf{v}^i , θ^i , ψ^i and p^i . The iterative process is stopped when, at each nodal point,

$$\|\mathbf{v}^i - \mathbf{v}^{i-1}\| + |\theta^i - \theta^{i-1}| + |\psi^i - \psi^{i-1}| \leq \varepsilon[\|\mathbf{v}^{i-1}\| + |\theta^{i-1}| + |\psi^{i-1}|], \quad (39)$$

where $\|\mathbf{v}\|^2 = v_r^2 + v_z^2$, and ε is a preassigned small number. Values of p^i are not included in equation (39) since p appears linearly in equation (32). The boundary condition (15) on the rod–cavity interface has been accounted for by the use of Lagrange multipliers.

4. COMPUTATION AND DISCUSSION OF RESULTS

The finite element code developed by Batra [11] and used to analyze steady state axisymmetric deformations of a viscoplastic target being penetrated by a rigid cylindrical penetrator was modified to solve the present problem. It employs six-noded triangular elements with v_r , v_z , θ and ψ approximated by piecewise continuous complete quadratic polynomials and p by piecewise linear polynomials. Within each element, p is expressed in terms of its values at the corner nodes, and other variables are expressed in terms of their values at all of the six nodes of the element. The absence of a diffusive term in equation (34) necessitates the use of either a superfine mesh or a fine mesh, with an artificial diffusive term included in equation (34) or the use of upwinding test functions [23]. The last technique is also referred to as the Petrov–Galerkin formulation [22]. Whereas Batra and Gobinath [24] used the Petrov–Galerkin formulation to study the steady-state penetration problem for compressible rigid–perfectly plastic targets, we follow Batra [11] and add a term

$$\delta \int_R \text{grad } \psi \cdot \text{grad } \xi \, dV$$

to the left-hand side of equation (34). Brooks and Hughes [25] have discussed in detail the justification for including such a term and have given equivalent ways of achieving the same objective.

We assume the penetrator to be made of a typical steel and take for it the following values of various material parameters:

$$\begin{aligned} n &= 0.01, & \psi_0 &= 0.017, & b &= 10^4 \text{ s}^{-1}, & m &= 0.025, & a &= 0.000555^\circ\text{C}^{-1}, \\ k &= 48 \text{ W m}^{-1} \text{ }^\circ\text{C}^{-1}, & c &= 473 \text{ J kg}^{-1} \text{ }^\circ\text{C}^{-1}, & \rho &= 7800 \text{ kg m}^{-3}, & \sigma_0 &= 180 \text{ MPa}, \\ h &= 20 \text{ W m}^{-2} \text{ }^\circ\text{C}^{-1}, & \tilde{h} &= 5 \text{ W m}^{-2} \text{ }^\circ\text{C}^{-1}, & r_0 &= 2.54 \text{ mm}, \\ \varepsilon &= 0.02, & \theta_a &= 0, & \tilde{\theta} &= 0, & \delta &= 2.4 \times 10^{-5}. \end{aligned}$$

This choice of values gives $\tilde{\theta}_0 = 48.9^\circ\text{C}$. However, we present below results in terms of non-dimensional quantities. We first investigate the effect of varying α , and then of different material models on the deformations of the rod.

Figure 2 depicts the computed velocity field for $\alpha = 5.0$ and the radius of the hemispherical bottom of the cavity equal to 2.5. The plotted velocity field clearly shows that the velocity at points on the free surface and the cavity wall are along the tangent to these surfaces. Thus the iterative technique [12] used to find the shape of the free surface, and the method of Lagrange multipliers employed to satisfy $\mathbf{v} \cdot \mathbf{n} = 0$ on the cavity wall, work quite well. Because of the presence of the advective term in equations (25) and (26), the finite element mesh had to be refined considerably as compared to that used in [12], where only the mechanical problem for a rigid–perfectly plastic rod striking the cavity defined by $z = 0.04r^4$ was analyzed. The finite element mesh shown in Fig. 1 and used in all of the work discussed herein has 7,865 nodes, as compared to 1,357 nodes in the earlier work [12]. A reason for changing the cavity shape from the parabolic one studied earlier to the hemispherical one being studied here is that the latter is closer to the shape of the target–penetrator interface found in the solution of the complete penetration problem in which both the target and the penetrator are presumed to be deformable; see e.g. Pidsley [26].

The velocity field for other values of α was found to be similar to that shown in Fig. 2. In Fig. 3 are shown the free surfaces for $\alpha = 3.3, 4.0$ and 5.0, and also the variation of the thickness of the outlet region with α . These results are strikingly different from those obtained in [12]. Whereas for the rigid–perfectly plastic rod studied in [12], the normal velocity at the outlet was very small as compared to the inlet speed of 1.0, such is not the case here. Consequently, the thickness of the outlet region is noticeably smaller for the present problem as compared to the one studied earlier. For the rigid–perfectly plastic rod, the thickness at the outlet increased significantly with an increase in the value of α ; in the present problem, the outlet thickness increases only slightly when α is varied from 3.3 to 5.0.

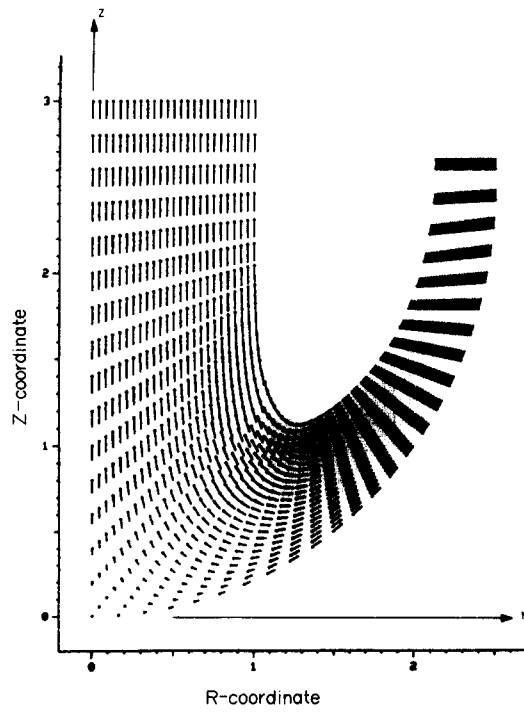


FIG. 2. The computed velocity field for $\alpha = 5.0$.

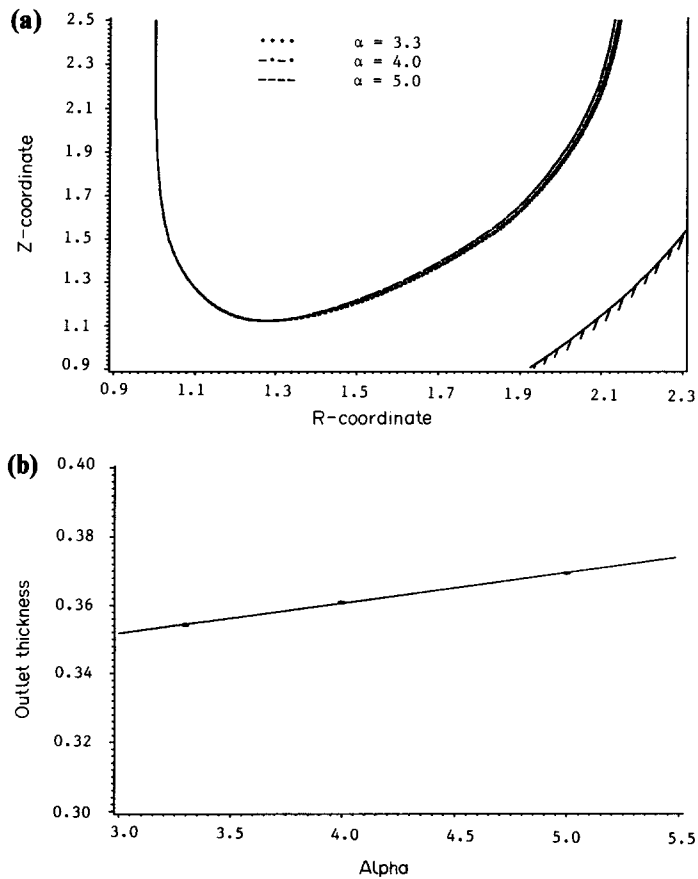


FIG. 3. (a) Shapes of the free surface for different values of α . (b) Thickness of the outlet region versus α .

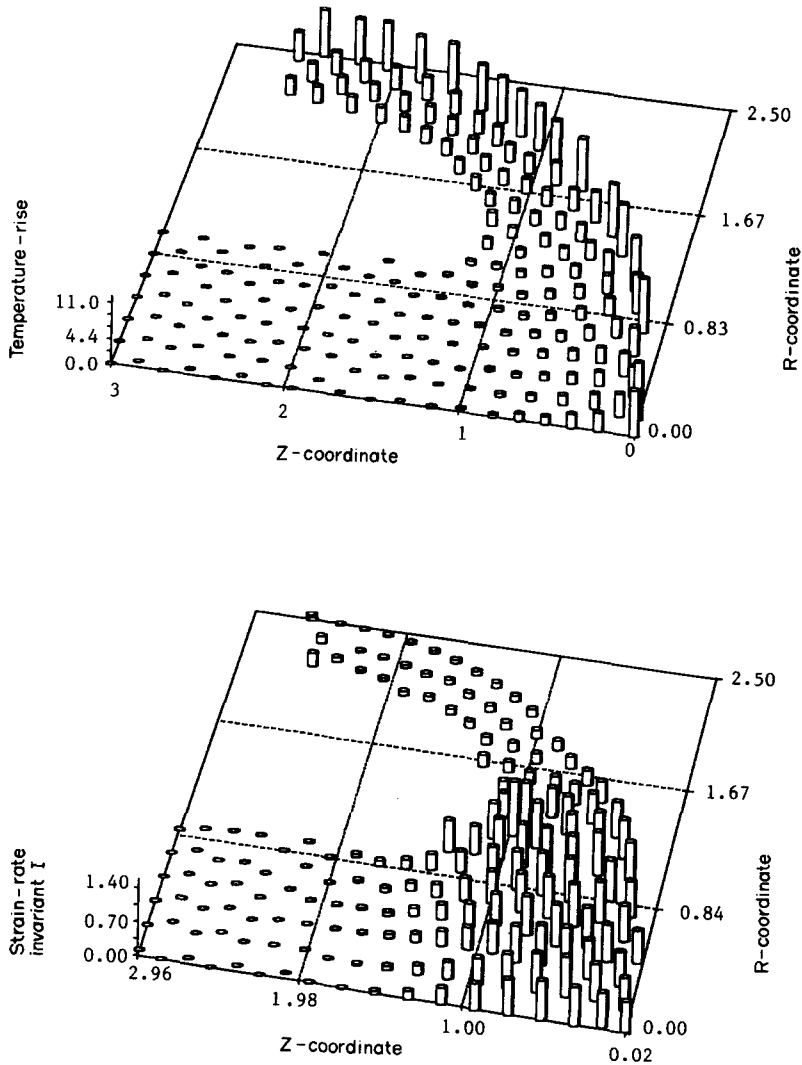


FIG. 4. Distribution of the strain-rate invariant I and temperature rise in the deforming region ($\alpha = 5.0$).

Figure 4 shows, for $\alpha = 5.0$, the distribution of the strain-rate invariant I and the temperature rise θ within the deforming region. It is obvious that significant deformations of the rod occur within the hemispherical region H of radius nearly 1.0 and centered at the bottom B (Fig. 1) of the cavity. Since the non-dimensional strain-rates ought to be multiplied by v_0/r_0 to get their dimensional counterparts, strain-rates of the order of 10^5 – 10^6 s^{-1} occur within this region. The strain-rate invariant I equals zero at the inlet and should be negligibly small near the outlet. Whereas for the rigid-perfectly plastic rod [12], the maximum value of I occurred near the bottom-most point E of the free surface, such is not the case here. At the stagnation point there is considerable heat generated due to plastic working and the temperature is high because of the very small value of the thermal diffusivity. Since the tangential velocity of the rod particles abutting the cavity wall increases slowly from 0 at the stagnation point to about 0.6 at $r = 1.5$, the transfer of heat by convection from the region near the stagnation point is also small. The plastic working and the heat generated thereby are appreciable at material particles within the hemispherical region H ; at material particles outside of this region and on the outlet side, the temperature rise is mainly due to the transport phenomenon and—to a lesser extent—the conduction of heat. The maximum temperature found to occur at any point is 504°C , which equals nearly one-third of the presumed melting temperature of the rod material.

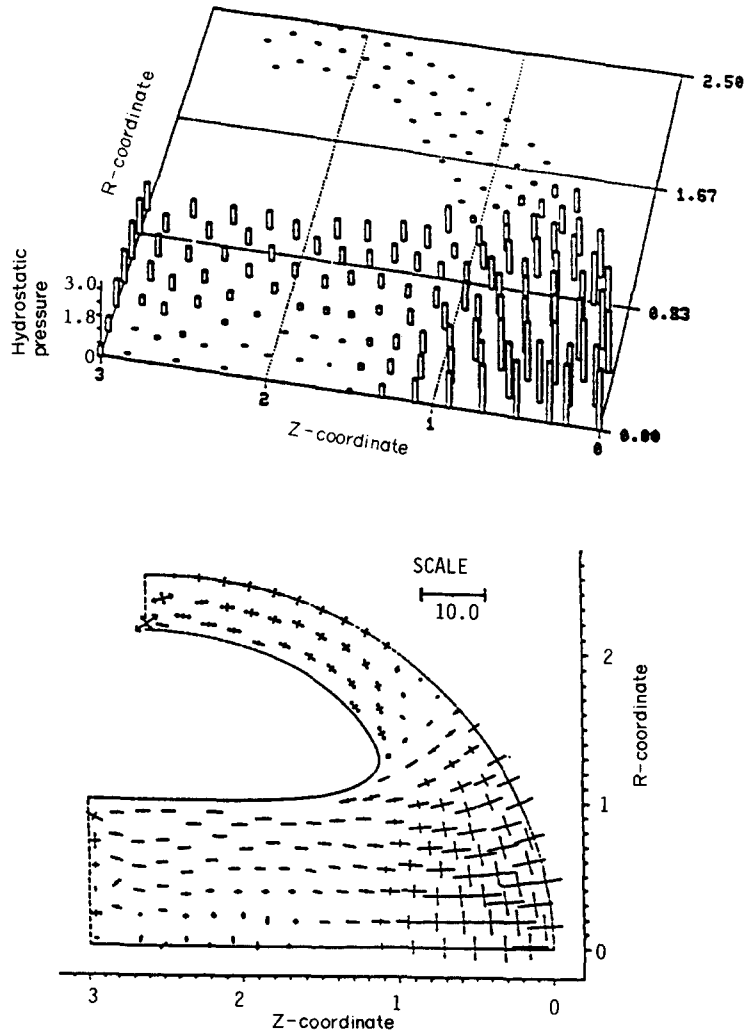


FIG. 5. Distribution of the principal stresses and the hydrostatic pressure in the deforming region ($\alpha = 5.0$).

The spatial distribution of the work-hardening parameter ψ is very similar to that of the temperature rise θ shown in Fig. 4. This is to be expected, since the equation governing the evolution of ψ is virtually identical to that of θ . Recall that we added the term

$$\delta \int_R \text{grad } \psi \cdot \text{grad } \xi \, dV$$

to the left hand side of equation (34). The computed value of ψ at any point is found to be a little less than that of θ because of the slightly smaller source term for ψ .

We have plotted in Fig. 5 the distribution of the principal stresses and the hydrostatic pressure in the deforming region. The lines are directed along the axes of principal stresses, and their lengths are proportional to the magnitudes of the principal stresses. The arrows at the ends of a line signify that the corresponding principal stress is tensile; otherwise it is compressive. Because of the high values of the hydrostatic pressure and the strain-rate invariant I in the hemispherical region H defined above, the magnitudes of the principal stresses at points in H are considerably more than that at points outside H. We should add that points near the cavity wall, which appear to be on the bounding surface and seemingly imply that the boundary condition of zero tangential traction on the wall is not well satisfied, are really a small distance away from the cavity surface. The presence of small tensile stresses on the exit side suggests that the incoming speed of the rod is not

high enough for the deformed material to be pushed out completely. Thus, at this striking speed, the head of the rod will very probably be upset into a mushroom shaped region. Recall that strain-rates at points in the vicinity of the inlet and outlet regions are negligibly small. The calculation of stresses at these points, according to equation (7), therefore involves the multiplication of and division by small numbers. Accordingly, the computed values of stresses near the inlet and the outlet region are not very reliable. This is one possible explanation for the small tensile stresses at isolated points near the inlet and rather large tensile stresses near a corner at the outlet. The high value of the hydrostatic pressure at the inlet is also an artifact of the numerical technique employed rather than a representation of any real phenomenon. These limitations notwithstanding, the computed values are meaningful in the severely deforming region near the bottom of the cavity.

That there is a tendency for the material particles to leave the cavity wall near the outlet region is evident from the computed positive values of the normal traction at these points. The normal and axial tractions at different points on the cavity wall are plotted in Fig. 6, where the arc length is measured from the bottom-most point B (cf. Fig. 1) of the cavity. As one would expect, the point where the separation tends to occur first moves outwards with an increase in α . Note that the axial traction computed at points for which the arc length exceeds 2 is quite small and, therefore, the contribution to the total axial force from points where flow separation seems to occur is insignificant. This is due to the fact that the cavity surface near the outlet is nearly parallel to the rod axis. As observed earlier, rod particles within a distance of r_0 from point B undergo severe deformations.

As for the rigid-perfectly plastic rod [12], the total axial force F , found to be given by $F = -1.848 + 1.569\alpha$, $3 \leq \alpha \leq 5$, depends rather strongly upon α in the present problem too. This was not so for the deformable viscoplastic target [11] being penetrated by a rigid cylindrical rod. In that problem, the computed axial force depended strongly upon the penetrator nose shape. In a real penetration problem, both the target and the penetrator materials deform, and the shape of the target-penetrator interface very probably changes with α . In the approximate theory of Tate [1, 2], the axial force acting on the target-penetrator interface is presumed to be constant. Because of the lack of availability of the experimental data in the open literature, it is hard to assess the range of validity of the computed results.

We now investigate the effect of different material models. The shapes of the free surfaces plotted in Fig. 7 show that there is an immense change in going from rigid-perfectly plastic

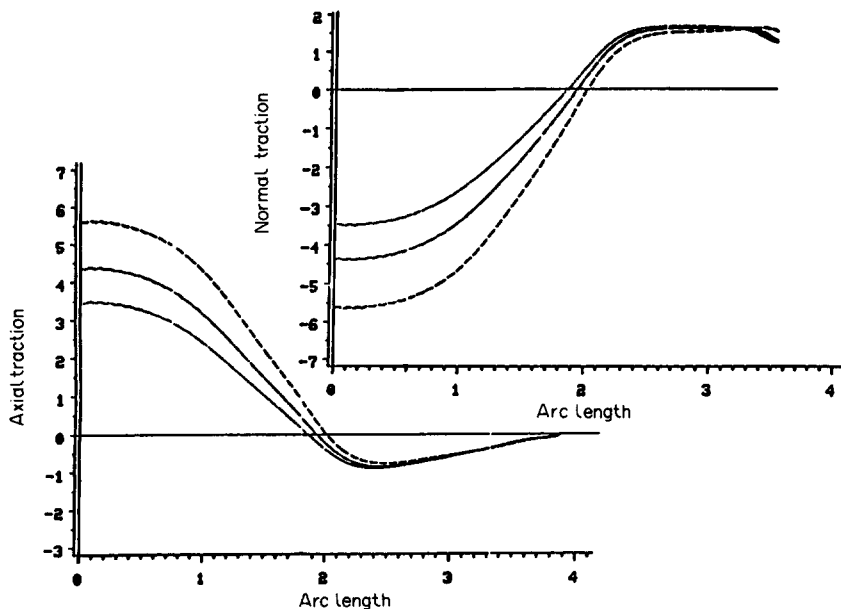


FIG. 6. Variation of the normal and axial tractions on the cavity wall.

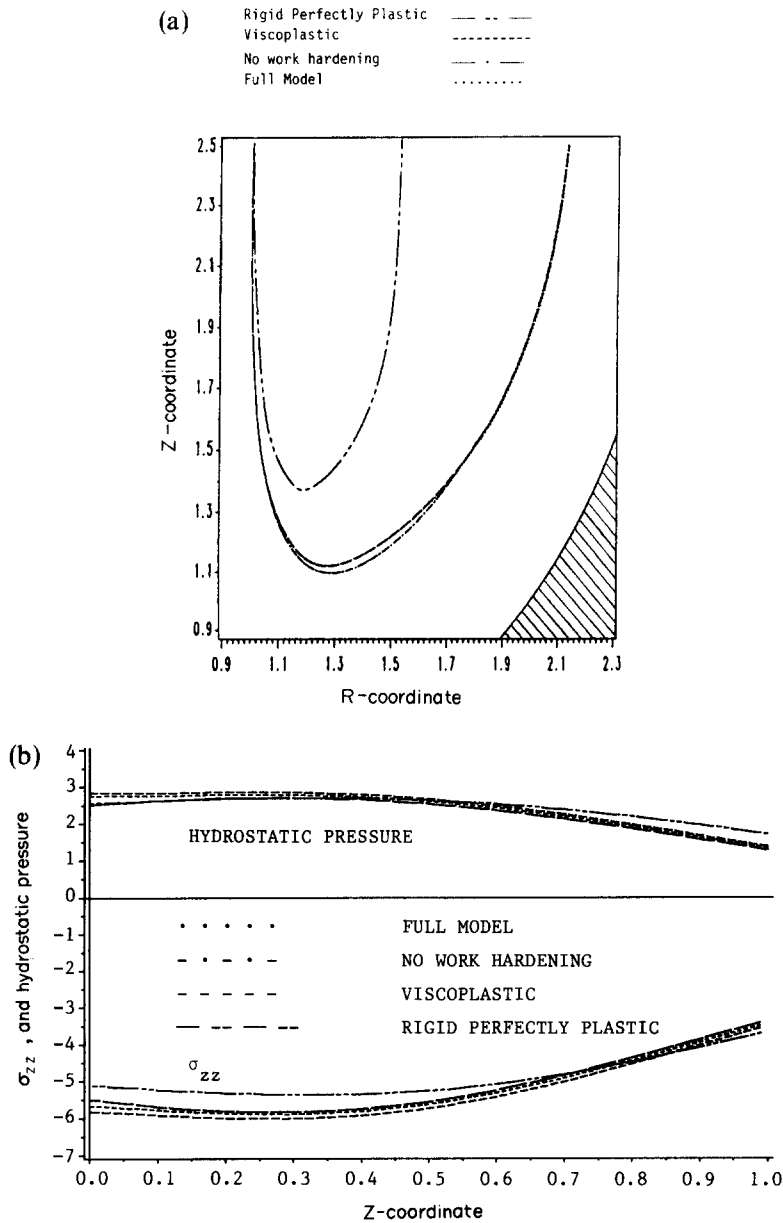


FIG. 7. (a) Free surfaces for four different material models. (b) Variation of the hydrostatic pressure and σ_{zz} on the axis of symmetry.

material to the viscoplastic material, and that the additional consideration of thermal softening alters the free surface only slightly near the bottom-most point. The free surface for the complete model virtually coincides with that when the rod material is modeled as viscoplastic with no work-hardening and no thermal softening. Recalling that the rigid-perfectly plastic material model is obtained from equation (10) by setting $b = 0$, $n = 0$ and $\gamma = 0$, we are now exploring whether the computed sharp change in the free surface profiles for $b = 0$ and $b = 10^4 \text{ s}^{-1}$ depends continuously upon b or whether there is a singular behavior at $b = 0$. Results plotted in Fig. 7(b) show that on the axis of symmetry and for $0 \leq z \leq 1.0$, the hydrostatic pressure does not depend that much on the material model used. However, the material model does noticeably affect the values of σ_{zz} , especially for $0 \leq z \leq 0.5$. On the axial line, uniaxial strain conditions prevail, approximately. Thus the magnitude of the deviatoric stress s_{zz} should equal $2/3$ the effective flow stress σ_e , which

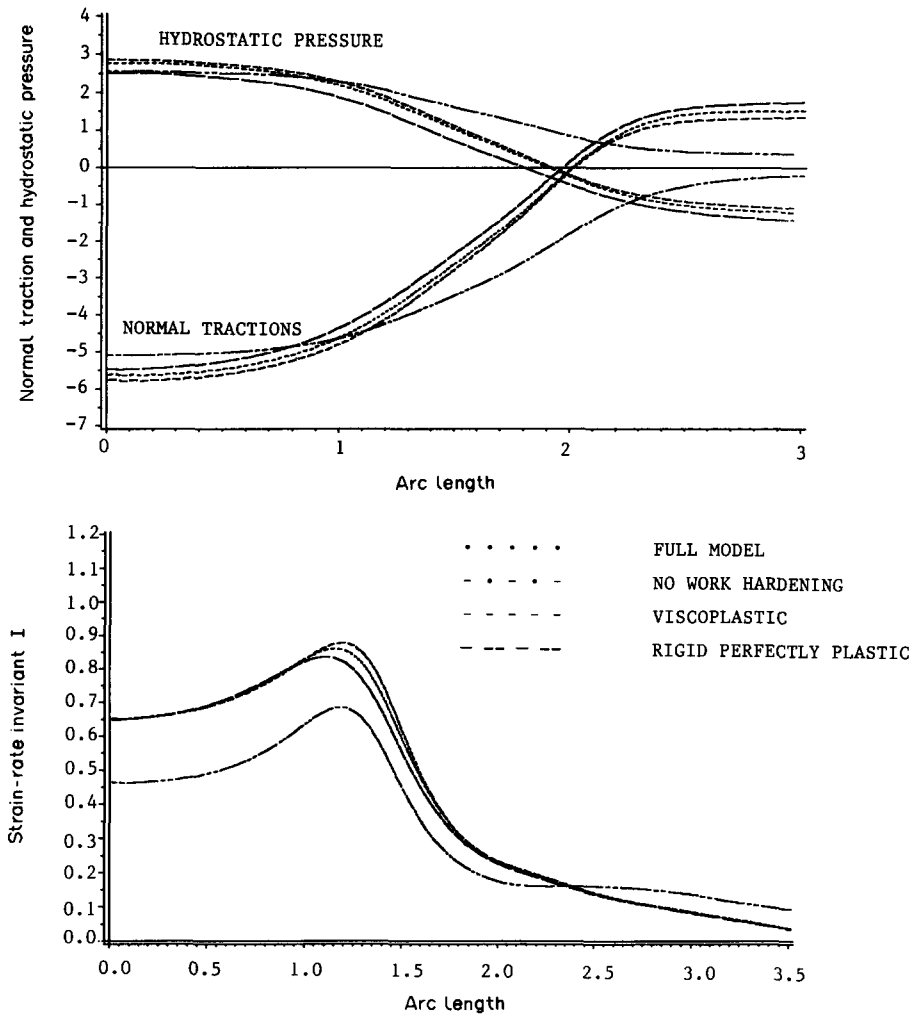


FIG. 8. Distribution of normal tractions, hydrostatic pressure and the strain-rate invariant on the cavity wall for four different material models.

equals $\sqrt{3}$ times the right-hand side of equation (13). The computed results satisfy $s_{zz} = (2/3)\sigma_e$ reasonably well, the difference being less than 5% for $0 \leq z \leq 0.50$.

It is quite obvious from the distribution of normal tractions on the cavity wall plotted in Fig. 8 that there is no separation of the material from the cavity wall for the rigid-perfectly plastic material. The consideration of strain-rate effects makes the material stiffer, and the striking speed of the rod is not large enough to push out completely all of the material deformed severely at the bottom of the cavity. The incorporation also of the work hardening and thermal softening effects has a less noticeable effect on the normal tractions at the cavity wall. The distribution of the hydrostatic pressure on the cavity wall shows that the point where the material tends to separate from the wall is close to the point where the hydrostatic pressure changes sign. For all four material models, the strain-rate invariant I increases slowly, takes on a maximum value when the arc length equals 1.3 and then drops rather quickly. The peak value of I occurs at a point near the bottom-most point of the free surface. It is clear that the values of I on the cavity wall are affected significantly by the consideration of strain-rate effects but little by the additional incorporation of work-hardening and/or thermal softening.

We realize that the maximum value 5 of α considered here is not high enough to solve strictly the problem we had set out to investigate. The three possible alternatives are to increase α , to change the cavity shape or to change the boundary conditions on the rod

material adjoining the cavity wall near the outlet. The last option requires finding shapes of two free surfaces, not an arduous but certainly a time consuming task unless one has a very robust algorithm to find the free surface. In spite of this shortcoming, the computed results are quite meaningful within the hemispherical region of radius 1.0 centered around the bottom of the cavity. Note that strain-rates near the inlet and the outlet regions are negligibly small, ensuring that the finite region studied is adequate.

5. CONCLUSIONS

The computed results show that during steady state deformations of a thermoviscoplastic rod striking a rigid hemispherical cavity, the axial force experienced by the rod depends strongly upon α . We recall that the non-dimensional parameter α , defined by equation (22), equals $\rho v_0^2 / \sigma_0$. The most severe deformations occur in the region between the cavity bottom and the bottom-most point on the free surface. The peak values of the non-dimensional strain-rate invariant I are found to be 1.034, 1.111 and 1.175 for $\alpha = 3.3, 4.0$ and 5.0, respectively, implying thereby that I depends weakly upon α . That is not to say that the dimensional values of I are weak functions of α , since the scaling factor v_0/r_0 between the two involves α . The point on the cavity wall where the flow has a tendency to separate from the cavity surface moves away from the axis of the rod as the striking speed is increased. For fixed values of α , the consideration of strain-rate hardening effects causes the separation of the rod material from the cavity wall. The maximum temperature of 504°C for $\alpha = 5$ and the full material model has been found to occur at (0.12, 0.003), which is located a small distance away from the stagnation point.

Acknowledgements—This work was supported by the U.S. Army Research Office Contract DAAG 29-85-K-0238 to the University of Missouri–Rolla. R. C. Batra is indebted to Drs T. W. Wright and John Walter, Jr of the U.S. Army Ballistic Research Laboratory for their suggestion that we consider a hemispherical cavity. Some of the computations were performed on the NSF sponsored supercomputer center at the University of Illinois–Urbana.

REFERENCES

1. A. TATE, A theory for the deceleration of long rods after impact. *J. Mech. Phys. Solids* **15**, 387–399 (1967).
2. A. TATE, Further results in the theory of long rod penetration. *J. Mech. Phys. Solids* **17**, 141–150 (1969).
3. V. P. ALEKSEEVSKII, Penetration of a rod into a target at high velocity. *Comb. Expl. Shock Waves* **2**, 63–66 (1966).
4. T. W. WRIGHT, A survey of penetration mechanics for long rods. In *Lecture Notes in Engineering*, Vol. 3, *Computational Aspects of Penetration Mechanics* (Edited by J. CHANDRA and J. FLAHERTY). Springer-Verlag, New York (1983).
5. M. E. BACKMAN and W. GOLDSMITH, The mechanics of penetration of projectiles into targets. *Int. J. Engng Sci.* **16**, 1–99 (1978).
6. C. E. ANDERSON, JR and S. R. BODNER, The status of ballistic impact modeling. *Int. J. Impact Engng* **7**, 9–35 (1988).
7. M. RAVID and S. R. BODNER, Dynamic perforation of viscoplastic plates by rigid projectiles. *Int. J. Engng Sci.* **21**, 577–591 (1983).
8. M. RAVID, S. R. BODNER and I. HOLCMAN, Analysis of very high speed impact. *Int. J. Engng Sci.* **25**, 473–482 (1987).
9. R. C. BATRA and T. W. WRIGHT, Steady state penetration of rigid–perfectly plastic targets. *Int. J. Engng Sci.* **24**, 41–54 (1986).
10. R. C. BATRA, Steady state penetration of viscoplastic targets. *Int. J. Engng Sci.* **25**, 1131–1141 (1987).
11. R. C. BATRA, Steady state penetration of thermoviscoplastic targets. *Comput. Mech.* **3**, 1–12 (1988).
12. R. C. BATRA and PEI-RONG LIN, Steady state deformations of a rigid–perfectly plastic rod striking a rigid cavity. *Int. J. Engng Sci.* **26**, 183–192 (1988).
13. W. D. FARREN and G. I. TAYLOR, The heat developed during plastic extrusion of metal. *Proc. R. Soc. Lond.* **A107**, 422–429 (1925).
14. J. F. BELL, *Physics of Large Deformation of Crystalline Solids*. Springer-Verlag, New York, Berlin, Heidelberg (1968).
15. U. S. LINDHOLM and G. R. JOHNSON, Strain-rate effects in metals at large strain-rates. In *Material Behavior Under High Stresses and Ultrahigh Loading Rates* (Edited by V. WEISS), pp. 61–79. Plenum Press, New York (1983).

16. Z. ROSENBERG, D. DAWICKE, E. STRADER and S. BLESS, High temperature experiments with a split Hopkinson bar using an induction heating technique. Report-UDR-TM-85-13, University of Dayton Research Inst. Impact Physics Lab., Dayton, Ohio (1985).
17. L. S. COSTIN, E. E. CRISMAN, R. H. HAWLEY and J. DUFFY, On the localization of plastic flow in mild steel tubes under dynamic torsion loading. *Inst. Phy. Conf. Ser.* No. 47, 90–100 (1979).
18. O. C. ZIENKIEWICZ, E. ONATE and J. C. HEINRICH, A general formulation for coupled thermal flow of metals using finite elements. *Int. J. Num. Meth. Engng* 17, 1497–1514 (1981).
19. A. TATE, A theoretical estimate of temperature effects during rod penetration. 9th Ballistic Symposium, pp. 2/307–2/314 (1987).
20. E. BECKER, G. CAREY and J. T. ODEN, *Finite Elements—An Introduction*. Prentice-Hall, Englewood Cliffs (1982).
21. O. C. ZIENKIEWICZ, *The Finite Element Method*. McGraw-Hill, London (1977).
22. T. J. R. HUGHES, *The Finite Element Method: Linear Static and Dynamics Finite Element Analysis*. Prentice-Hall, Englewood Cliffs (1987).
23. J. C. HEINRICH, P. S. HUYANKORN, O. C. ZIENKIEWICZ and A. R. MITCHELL, An 'upwind' finite element scheme for two-dimensional convective-transport equation. *Int. J. Num. Meth. Engng* 11, 131–148 (1977).
24. R. C. BATRA and T. GOBINATH, Steady state penetration of compressible rigid–perfectly plastic targets. *Int. J. Engng Sci.* 26, 741–751 (1988).
25. A. N. BROOKS and T. J. R. HUGHES, Streamline upwind/Petrov–Galerkin formulations for convection dominated flows with particular emphasis on the incompressible Navier–Stokes equations. *Comput. Meths appl. Mech. Engng* 32, 199–259 (1982).
26. P. H. PIDSLEY, A numerical study of long rod impact onto a large target. *J. Mech. Phys. Solids* 32, 315–333 (1984).